

Anhydride Post-Synthetic Modification in a Hierarchical Metal-Organic Framework

Shoushun Chen, zhongxin song, Jinghui Lyu, Ying Guo, Bryan E.G. Lucier, Wilson Luo, Mark S. Workentin, Xueliang Sun, and Yining Huang

J. Am. Chem. Soc., **Just Accepted Manuscript** • DOI: 10.1021/jacs.9b13414 • Publication Date (Web): 09 Feb 2020

Downloaded from pubs.acs.org on February 9, 2020

Just Accepted

“Just Accepted” manuscripts have been peer-reviewed and accepted for publication. They are posted online prior to technical editing, formatting for publication and author proofing. The American Chemical Society provides “Just Accepted” as a service to the research community to expedite the dissemination of scientific material as soon as possible after acceptance. “Just Accepted” manuscripts appear in full in PDF format accompanied by an HTML abstract. “Just Accepted” manuscripts have been fully peer reviewed, but should not be considered the official version of record. They are citable by the Digital Object Identifier (DOI®). “Just Accepted” is an optional service offered to authors. Therefore, the “Just Accepted” Web site may not include all articles that will be published in the journal. After a manuscript is technically edited and formatted, it will be removed from the “Just Accepted” Web site and published as an ASAP article. Note that technical editing may introduce minor changes to the manuscript text and/or graphics which could affect content, and all legal disclaimers and ethical guidelines that apply to the journal pertain. ACS cannot be held responsible for errors or consequences arising from the use of information contained in these “Just Accepted” manuscripts.

Anhydride Post-Synthetic Modification in a Hierarchical Metal-Organic Framework

Shoushun Chen,^{a¶} Zhongxin Song,^{b,c¶} Jinghui Lyu,^{a,d} Ying Guo,^{a,e} Bryan E.G Lucier,^a Wilson Luo,^a Mark S. Workentin,^a Xueliang Sun^{*b} and Yining Huang^{*a}

^a *Department of Chemistry, The University of Western Ontario, London, Ontario, Canada N6A 5B7.*

^b *Department of Mechanical and Materials Engineering, The University of Western Ontario, London, Ontario, Canada N6A 5B9*

^c *College of Materials Science and Engineering, Shenzhen University, Shenzhen 518060, China*

^d *College of Chemical Engineering, Zhejiang University of Technology, State Key Laboratory Breeding Base of Green Chemistry Synthesis Technology, Hangzhou, PR China, 310032.*

^e *State Key Laboratory of Chemical Resource Engineering, Beijing University of Chemical Technology, P.O. Box 98, Beijing, PR China, 100029.*

¶ These authors contributed equally to this work.

* Corresponding authors; Y.H. Email: yhuang@uwo.ca, X.S. Email: xsun@eng.uwo.ca

Abstract

Metal-organic frameworks (MOFs) are important porous materials. Post-synthetic modification (PSM) of MOFs via the pendant groups or secondary functional groups of organic linkers has been widely used to introduce new, or enhance existing properties of MOFs for various practical applications. In this work, we have constructed, for the first time, a novel platform for PSM of MOFs by introducing anhydride functional group into a hierarchically porous MOF (MIL-121) as an effective anchor. We have demonstrated that the combination of the high reactivity of anhydride and hierarchical porosity makes this protocol particular novel and important as it led to excellent opportunities of incorporating not only a wide variety of organic molecules with different sizes and chemical nature, but also the noble metal complexes in MOFs. Specifically, we show that the anhydride group decorated in the MOF exhibits a high reactivity towards covalently binding 10 different guest molecules including alcohols, amines, thiols and noble metal (Pt(II)/Pt(IV)) complexes, whereas the hierarchical pores created in the MOF allow the incorporation of guest species varying in size from methanol to larger molecules such as polyaromatic amines. This novel approach provides the community with a new avenue to prepare MOF-based materials for targeted applications. To illustrate this point, we furnish an example of using this new platform to prepare a Pt-based electrocatalyst which shows excellent catalytic activity towards the oxygen reduction reaction (ORR), a pivotal half-reaction in hydrogen-oxygen fuel cells and other energy storage devices.

Introduction

In the past two decades, metal-organic frameworks (MOFs) have emerged and grown as the largest branch of porous materials,¹ leading to numerous new materials with many applications including gas storage,²⁻³ gas separation,⁴ catalysis,⁵⁻⁷ chemical sensing,⁸ drug delivery,⁹⁻¹⁰ electrochemical energy storage and conversion.¹¹ MOFs are crystalline materials in which metal ions/clusters are connected via organic linkers to form three-dimensional porous frameworks. The robust structure and functionalization potential of organic components allow one to introduce diverse chemical functionalities into MOFs through post-synthetic modification (PSM) while keeping the overall MOFs topology intact.¹²⁻¹³ PSM has been employed as a general approach to improve the existing properties of and introduce new features to MOFs, with examples including enhancing framework stability to moisture, increasing gas adsorption capability, and introducing new catalytic sites.¹³⁻¹⁴

Among post-synthetic methods for MOFs,¹³⁻¹⁴ covalent modification of organic linkers via a pendant group of the linker or second functional group has been employed as an efficient approach.¹²⁻¹⁴ Although reported MOF entries in Cambridge Structural Database (CSD) have surpassed 70000,¹⁵ the available functional groups as targets for PSM are mainly limited to few organic species such as amino groups, hydroxyl groups, catechol, thiocatechol and 2,2'-bipyridyl moieties, etc.^{13-14, 16} The types of MOFs that are suitable for PSM are also limited.

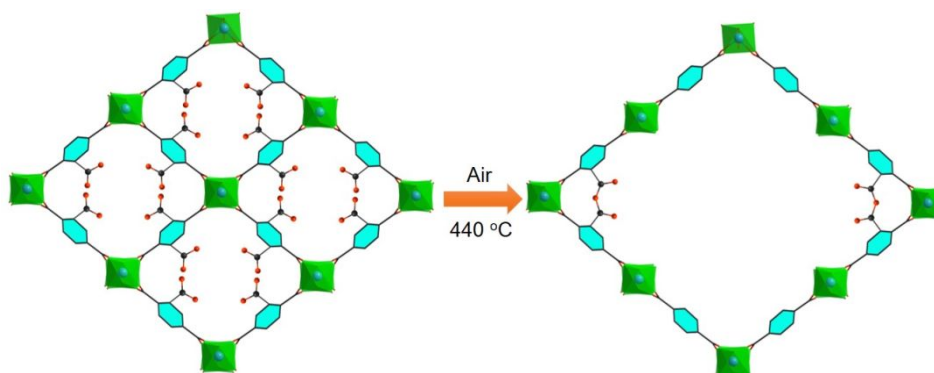
1
2
3
4 Factors limiting MOF selection for PSM include the stability of the MOF, as in
5
6 order to maintain the MOF topology and avoid severe structural damage, the MOF
7
8 candidate for PSM must be chemically robust. Preferred MOFs for PSM are
9
10 typically microporous zirconium MOFs due to their chemical stability, such as
11
12 UiO-66/67 and related materials.¹³ The pore size of MOFs is another key factor
13
14 of concern for PSM.¹⁴ Most MOFs have micropores with pore diameters less than
15
16 2 nm, which in many cases limits the mass transfer in the channels and prevents
17
18 the incorporation of large guest molecules.¹⁴ For PSM considerations, it is
19
20 important for MOFs to have sufficiently large pores that can encapsulate the
21
22 targeted guest species for desired applications.
23
24
25
26
27
28
29

30
31 Anhydrides are stable but reactive carboxylate derivatives that are widely used
32
33 in organic synthesis for making covalent bonds. For example, they are typically
34
35 used for acetylation of alcohols and amines in organic synthesis.¹⁷ Although
36
37 decorating MOFs with pendant anhydride groups via free carboxylic acid groups
38
39 on the linkers was reported in the literature,^{18,19} to the best of our knowledge,
40
41 anhydride formed inside hierarchically porous MOFs has not been used as an
42
43 anchor for PSM. In the present work, we demonstrate, for the first time, that an
44
45 anhydride grafted inside a MOF with a hierarchical pore system can be used as a
46
47 novel functional handle for PSM. The MOF chosen to highlight the efficacy of
48
49 anhydride functionality for PSM is MIL-121, an aluminum-based MOF
50
51 incorporating the low-cost linker precursor 1,2,4,5-benzenetetracarboxylic acid,
52
53 H₄BTEC. This MOF features two “free” uncoordinated carboxylic acid (COOH)
54
55
56
57
58
59
60

1
2
3
4 groups directed toward the interior of the channels, since only two of the four
5
6 COOH groups in the BTEC linker are coordinated to the metal centers (Scheme
7
8 1).¹⁸ These uncoordinated COOH groups occupy interior volume, thus MIL-121
9
10 has a limited pore aperture¹⁸ and very small Brunauer-Emmauer-Teller (BET)
11
12 surface area. Very recently, we reported that the formation of anhydride groups
13
14 and creation of a hierarchical pore system within MOF MIL-121 can be achieved
15
16 simultaneously in a controlled fashion via thermolysis.¹⁹
17
18
19
20
21
22

23 In the present PSM study, using the novel platform built on the thermally
24
25 treated hierarchically porous MIL-121 (termed HMIL-121) decorated with
26
27 anhydride, we have successfully grafted 10 different organic/inorganic species in
28
29 HMIL-12. Specifically, we demonstrate that the combination of reactive
30
31 anhydride groups and a hierarchical pore system permits immobilization of a
32
33 variety of organic molecules, including alcohols, amines and thiols, ranging in
34
35 size from small molecules such as methanol to relatively large organic compounds
36
37 such as polyaromatic amines. We also show that the inorganic Pt complex,
38
39 tetraamine platinum hydroxide, can also be successfully incorporated into HMIL-
40
41 121, demonstrating that anhydrides formed in the MOF pores can be used not only
42
43 for introduction of a variety of organic moieties, but also for metalation with noble
44
45 metals. These PSM processes only require a one-step treatment, and the Pt
46
47 complex incorporation proceeds at room temperature in water without any added
48
49 catalyst, showing that the anhydride is an effective PSM anchor site. HMIL-121
50
51 has been functionalized via anhydride groups with a variety of organic and
52
53
54
55
56
57
58
59
60

1
2
3
4 inorganic compounds, and thoroughly characterized using nitrogen adsorption
5 isotherms, powder X-ray diffraction (PXRD), scanning electron microscopy
6 (SEM), X-ray photoelectron spectroscopy (XPS) and ^1H , ^{13}C , and ^{195}Pt solid-state
7 NMR (SSNMR) spectroscopy. The information obtained in this study unlocks a
8 better understanding of the chemistry underlying the PSM process. To
9 demonstrate the potential for using the PSM protocol described in this work to
10 prepare MOF-based materials with practical applications, we employ a treatment
11 to transform the above-mentioned Pt-loaded HMIL-121 to a conductive
12 electrocatalyst that exhibits excellent catalytic activity towards the oxygen
13 reduction reaction (ORR).
14
15
16
17
18
19
20
21
22
23
24
25
26
27
28
29



44 **Scheme 1.** A depiction of the conversion from microporous MIL-121 to a hierarchically porous
45 MOF with decorated anhydride groups under a high temperature of 440 °C in the air. During
46 thermal treatment, the local structure partly collapses, yielding expanded pores. Concomitantly,
47 the dangling free carboxylic acid groups pointing towards the interior of the channel are
48 condensed to form anhydride groups. Color code: black, C; red, O; and the center green
49 octahedron represents AlO_6 .
50
51
52
53
54
55

56 Experimental Section

57 Sample preparation

1
2
3
4 **MIL-121** was prepared based on a previously reported procedure with some
5
6 modifications.¹⁸ A mixture of 1.80 g $\text{Al}(\text{NO}_3)_3 \cdot 9\text{H}_2\text{O}$ (Alfa Aesar, 98 %) and 0.60
7
8 g pyromellitic acid (1,2,4,5-benzenetetracarboxylic acid (BTEC), Alfa Aesar,
9
10 96 %) was dissolved in 10.0 mL of deionized H_2O . After stirring the reagent
11
12 mixture for 10 min, 0.5 mL 4.0 M HCl was added. After stirring for another 5
13
14 min, the mixture was placed in a Teflon chamber within a Teflon-lined stainless
15
16 steel autoclave. The autoclave was then sealed and heated in an oven at 210 °C
17
18 for 16 h. After cooling the autoclave to room temperature, a white powder of as-
19
20 made MIL-121 was obtained by centrifugation and dried in an oven at 90 °C for
21
22 5 h.
23
24
25
26
27
28
29

30 **Solvent exchanged MIL-121.** According to reference 18, the pores of as-made
31
32 MIL-121 contain unreacted linkers from MOF synthesis. Therefore, a methanol
33
34 (MeOH)-based solvent exchange procedure was carried out to remove unreacted
35
36 BTEC ligands. A mixture of 0.20 g as-made MIL-121 and 20.0 mL of methanol
37
38 was placed into a Teflon container within a Teflon-lined stainless steel autoclave,
39
40 which was then heated in an oven at 150 °C for 24 h. Upon cooling, the MeOH
41
42 solvent was decanted and replaced with fresh MeOH. This solvent exchange
43
44 process was repeated twice every 24 hours. The final product was then dried in an
45
46 oven at 90 °C for 1 h and referred to as MIL-121.
47
48
49
50
51
52

53 **Hierarchically porous MIL-121.** Hierarchically porous MIL-121 was obtained
54
55 by following the documented procedure:¹⁹ a MIL-121 sample was placed in an
56
57 oven at 440 °C and heated for 16 h. During this process, decarboxylation occurred
58
59
60

1
2
3
4 and some metal centers were eliminated from the framework, creating hierarchical
5
6 pores inside the MOF featuring grafted anhydride groups. The resulting MOF is
7
8 termed as HMIL-121, which was then used as the starting material for post-
9
10 synthetic modification (PSM).
11

12
13
14 **Acetylation (*i.e.* esterification) by alcohols.** The esterification of HMIL-121
15
16 decorated with anhydride groups via methanol is described here in detail as an
17
18 example. The acetylation details of the rest of the compounds can be found in the
19
20 SI.
21
22

23
24
25 **MeO-HMIL-121.** A mixture of 200.0 mg HMIL-121 and 10.0 mL 99.9% MeOH
26
27 (Fisher Chemical) was placed in a 25 mL round-bottom flask and then 3 drops of
28
29 concentrated H₂SO₄ (98%, ACP chemicals) were added. The reagent mixture in a
30
31 flask was heated in an oil bath at 60 °C. The reaction was held for 5 hours under
32
33 magnetic stirring. The product was isolated by centrifugation. To remove residual
34
35 MeOH, the sample was immersed within 25 mL of DI water and stirred for 5 min
36
37 in a 50.0 mL centrifuge tube. This washing process was repeated three times
38
39 before the collected product was dried at 90 °C. The dried sample was completely
40
41 activated at 150 °C under dynamic vacuum (≤ 1 mbar) for *ca.* 8 h; the fully
42
43 activated final product is termed MeO-HMIL-121.
44
45
46
47
48
49

50 51 **Powder X-ray diffraction (PXRD)**

52
53
54 PXRD patterns were recorded on an Inel CPS powder diffractometer
55
56 operating using Cu K α radiation ($\lambda = 1.5406$ Å). The reflections were collected at
57
58 2θ values ranging between 5 and 120° using an increment of 0.02°.
59
60

N₂ adsorption measurements

N₂ adsorption isotherms were measured using a Micromeritics ASAP 2020 porosity analyzer at a temperature of 77 K.

Electron microscopy

All SEM images were taken on a scanning electron microscope (Hitachi S-4800) operating at 5 kV. TEM samples were prepared by drop-casting an ultrasonicated solution of dilute high-performance liquid chromatography grade methanol solution with the sample of interest onto a lacey carbon grid. TEM and high-resolution TEM (HRTEM) images were taken on a JEOL 2010F Transmission Electron Microscope equipped with an energy dispersive spectrometer (EDS).

Thermogravimetric analysis (TGA)

TGA was carried out on a TA Instruments Q50 thermogravimetric instrument under N₂ flow (40 mL·min⁻¹) with heating from 40-800 °C at a rate of 10 °C·min⁻¹.

ICP-OES

The Pt loading level in HMIL-121-900 was determined by inductively coupled plasma-optical emission spectroscopy (ICP-OES). 10.0 mg of Pt-HMIL-121-900 was dispersed in 10.0 mL aqua regia (HCl:HNO₃ = 3:1) to completely dissolve Pt nanoparticles dispersed in the MOF-based matrix overnight. Then, 1.0 mL of aqua regia with dissolved Pt was diluted with 9.0 mL H₂O and the resulting solution was used to measure the Pt concentration by ICP-OES. From ICP analysis, the Pt loading in Pt-HMIL-121-900 was determined to be 7.0 wt%.

SSNMR measurement

All ^1H , ^{13}C , and ^{195}Pt SSNMR experiments were performed at a magnetic field of 9.4 T using a Varian InfinityPlus wide-bore NMR spectrometer.

^{13}C and ^1H SSNMR spectroscopy. ^{13}C and ^1H SSNMR spectra [$\nu_0(^{13}\text{C}) = 100.5$ MHz, $\nu_0(^1\text{H}) = 399.5$ MHz] were referenced to TMS using adamantane as a secondary reference. Specifically, the high-frequency ^{13}C signal at 38.57 ppm and the ^1H resonance at 1.85 ppm were used for the secondary referencing.²⁰⁻²¹ ^1H - ^{13}C cross-polarization magic angle spinning (CP/MAS) experiments were performed with proton decoupling and a spinning frequency of 14 kHz using a spectral width of 100 kHz, along with a ^1H 90° pulse length of 4.5 μs , a contact time of 7 ms and a recycle delay of 3 s. ^1H MAS experiments were performed at a spinning frequency of 14 kHz and a spectral width of 100 kHz, utilizing a 90° pulse of 4.5 μs and a recycle delay of 2 s. For each ^1H spectrum, 4 scans were collected. The number of scans for each ^{13}C spectrum are listed as follows, in the format of *sample : number of scans*: MeO-HMIL-121:4785; EtO-HMIL-121:7785; 2-PE-HMIL-121:6897; MeNH-HMIL-121:3768; aniline-HMIL-121:6163; p-toludine-HMIL-121:8794; 4-ABP-HMIL-121:4308; 1-AP-HMIL-121:9428; EDT-HMIL-121:4578.

Static ^1H - ^{195}Pt BRAIN-CPMG SSNMR measurements. A 1.0 M aqueous Na_2PtCl_6 solution was used as a chemical shift reference ($\nu_0(^{195}\text{Pt}) = 85.59$ MHz, $\delta_{\text{iso}} = 0.0$ ppm).²² The ^{195}Pt spectra of the two samples (*i.e.* $\text{Pt}(\text{NH}_3)_4(\text{OH})_2$ and Pt-HMIL-121) were acquired using BRAIN-CPMG pulse sequence²³ with WURST-

80 excitation pulses²⁴⁻²⁵ and ¹H decoupling. The ¹H 90 ° pulse length was 3.75 μs and a contact time of 7 ms was used. The CP (cross polarization) - WURST sweep range was 500 kHz. The ¹H-¹⁹⁵Pt spectra of the two samples were produced by coaddition of several individual sub-spectra due to the wide spectral breadth. The ¹H-¹⁹⁵Pt BRAIN-CPMG spectrum of the Pt salt, Pt(NH₃)₄(OH)₂, was assembled by the coaddition of 8 sub-spectra. For each sub-spectrum, the pulse delay employed was 3 s, spectral window is 1000 kHz, spikelet separation in the frequency domain is 5000 Hz and number of scans is 500. The ¹⁹⁵Pt spectrum of Pt-HMIL-121 was constructed from the coaddition of 3 sub-spectra; for each sub-spectrum, the pulse delay was 1.65 s, spectral window is 1000 kHz, spikelet separation in the frequency domain is 9090 Hz and number of scans is 219992.

Electrochemical measurements

The electrochemical characterization was performed in a three-electrode system using a rotating-disk electrode (RDE) setup with an Autolab electrochemistry station and rotation control (Pine Instruments). The ink was prepared by mixing 3.0 mg of catalyst in 3.0 mL of aqueous solution containing 0.6 mL of isopropyl alcohol and 30 μL of Nafion (5.0 wt%). 30 min of sonication was conducted to ensure good dispersion and wetting of the catalyst. 60 μL of the catalyst ink was pipetted onto a polished glassy carbon electrode (Pine, 5.0 mm dia., 0.196 cm²) and allowed to dry at room temperature. All electrochemical measurements were carried out in 0.1 M HClO₄ electrolyte using a Pt wire as a

1
2
3
4 counter electrode and a reversible hydrogen electrode (RHE) as a reference
5
6 electrode. All potentials reported henceforth are *vs.* RHE. Each electrode was
7
8 activated by scanning from 0.05 to 1.1 V at 50 mV·s⁻¹ in N₂-saturated 0.1 M
9
10 HClO₄ solution until no change was observed in the cyclic voltammetry (CV)
11
12 curves. O₂ was then bubbled into the HClO₄ solution for 30 min to achieve an O₂-
13
14 saturated electrolyte. ORR linear sweep voltammetry (LSV, 10 mV·s⁻¹) was
15
16 conducted in O₂-saturated 0.1 M HClO₄ solution on the RDE system with a
17
18 rotation speed of 1600 rpm. The LSV curves obtained under N₂ were subtracted
19
20 from the LSV curves obtained under O₂ to remove the non-Faradaic current. For
21
22 comparison, the commercial 40% Pt/C catalyst was prepared on the electrode
23
24 using a similar procedure as described above with a Pt loading of 10 mg·cm⁻². The
25
26 kinetic current was calculated from the ORR polarization curves by using mass-
27
28 transport correction and normalized to the loading amount of Pt in order to
29
30 compare the mass activity of different catalysts. The calculations were based on
31
32 the Levich-Koutecky equation:²⁶
33
34
35
36
37
38
39
40
41
42
43
44
45
46
47
48
49
50

$$1/i = 1/i_k + 1/i_d$$

51
52 Where i_k is the kinetic current and i_d is the diffusion-limiting current.
53
54

55 **Results and Discussion**

56 **Preparation and characterization of the materials used for PSM:** 57 **hierarchically porous MIL-121 decorated with anhydride groups** 58 59 60

1
2
3
4 The protocol for preparing hierarchically porous MIL-121 decorated with
5
6 anhydride functional groups via thermolysis was described in reference 19 and
7
8 details are given in the Experimental section and the SI. The hierarchial pores in
9
10 MIL-121, including the pore size and pore volume, can be finely tuned by
11
12 controlling the thermolysis temperature and duration. In the present study, unless
13
14 stated otherwise, all the hierarchically porous MIL-121 based materials with
15
16 anhydride groups used for PSM were obtained by thermolysis of MIL-121 at
17
18 440 °C for 16 hours, as we have found the materials prepared under these
19
20 conditions have the largest BET surface areas. Hereafter, these products are
21
22 referred to as HMIL-121.
23
24
25
26
27
28
29
30

31 The N₂ adsorption isotherm of a typical HMIL-121 sample is shown in Figure
32
33 S1a. The type IV isotherm indicates the existence of mesopores. The calculated
34
35 Brunauer-Emmett-Teller (BET) surface area is 887.6 m²/g, including a
36
37 microporous area of 623.8 m²/g and a mesoporous area of 263.8 m²/g. The
38
39 material has an average pore size of 5.20 nm. The pore size distribution in HMIL-
40
41 121 was also calculated by the density functional theory (DFT) method and is
42
43 shown in Figure S1b, further confirming that mesopores are present in this MOF.
44
45 The SEM image of the HMIL-121 sample (Figure S1d) features mesopores of
46
47 various sizes. The existence of anhydride groups in HMIL-121 is directly
48
49 confirmed by ¹³C solid-state NMR (SSNMR) spectroscopy, which will be
50
51 discussed later.
52
53
54
55
56
57
58
59
60

Modification of HMIL-121 with alcohols and aromatic amines.

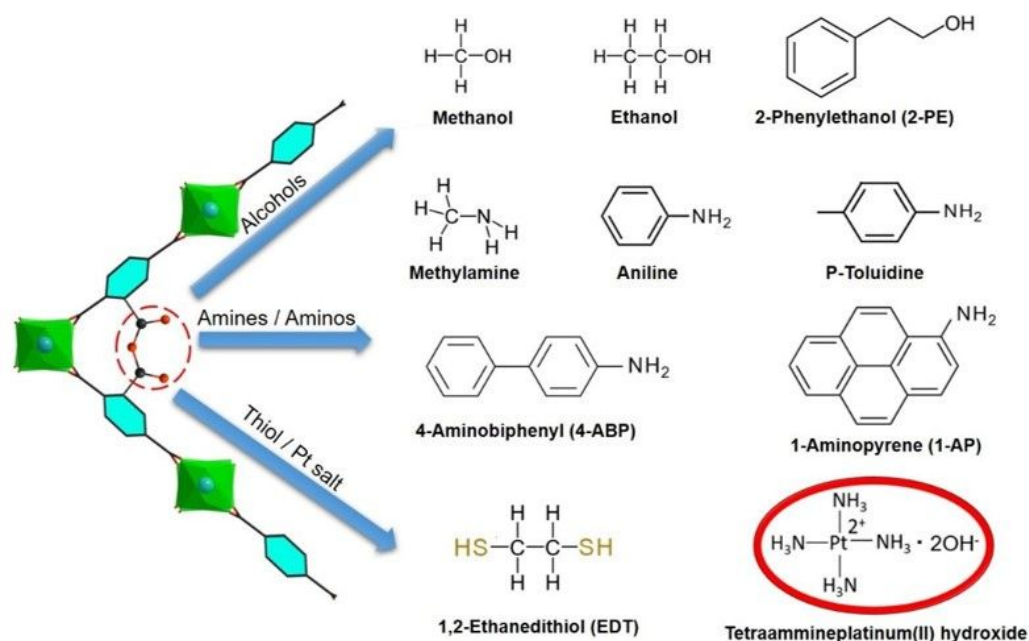


Figure 1. Illustration of the reactivities of anhydride groups in HMIL-121 towards different organic compounds and a platinum salt. (O red, C black, blue Al).

Nine different organic functional moieties and one platinum complex [methanol (MeOH), ethanol (EtOH), 2-phenylethanol (2-PE), methylamine (MeNH₂), aniline, *p*-toluidine, 4-aminobipenyl (4-ABP), 1-aminopyrene (1-AP), 1,2-ethyldithiol (EDT) and tetraamineplatinum(II) hydroxide] have been successfully immobilized inside the pores of HMIL-121 (Figure 1). The PSM procedures for introducing each guest species were individually optimized based on the chemical nature of each guest. The resulting PSM variants are termed in the format of “grafted species-HMIL-121;” *e.g.*, MeO-HMIL-121 corresponds to HMIL-121 functionalized by methanol with a methoxy group as the grafted

species. Details of PSM procedures can be found in the Experimental section and the SI. The powder X-ray diffraction (PXRD) patterns of HMIL-121 variants functionalized by PSM are very similar to pristine HMIL-121 (Figure S2), suggesting the long-range order and topology of the MOF are preserved after PSM. The N_2 gas adsorption isotherms of HMIL-121 and its PSM variants are given in Figure 2. The N_2 adsorption capacities of modified HMIL-121 variants all significantly decreased versus the parent HMIL-121 MOF, which results from reduced pore size/space due to the existence of incorporated guest species. This decrease in N_2 uptake is a clear marker of successful guest introduction into HMIL-121 via reaction with anhydride groups.

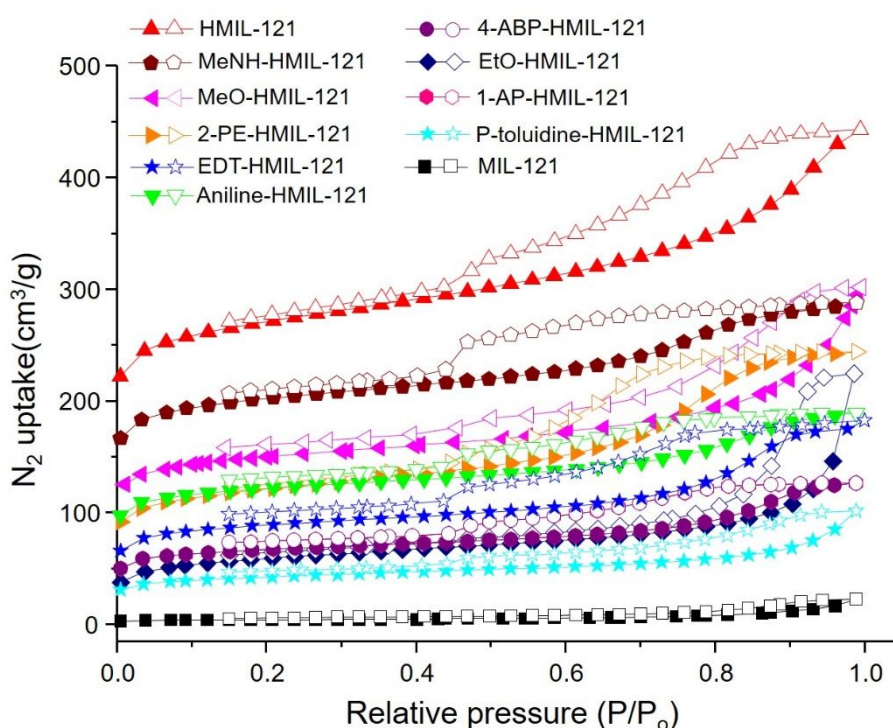


Figure 2. N_2 adsorption-desorption isotherms of MIL-121, HMIL-121 and post-synthetically modified HMIL-121 variants. Solid circles represent adsorption and open circles denote desorption measurement points.

1
2
3
4 The pore size distributions in MIL-121, HMIL-121 and post-synthetically
5 modified HMIL-121 variants have been calculated from the N₂ adsorption
6 isotherms via the DFT method, and are shown in Figure S3. The pore size
7 distribution of MIL-121 indicates that there are very little micropores or
8 mesopores in the sample. This near absence of MIL-121 porosity is due to the
9 steric hindrance of its dangling free carboxylate groups, which occupy and block
10 the pores.¹⁸⁻¹⁹ The DFT calculation indicates that after thermal treatment, HMIL-
11 121 features two different groups of pores: micropores with a size distribution
12 centered around 15 Å, and mesopores ranging from 20 Å to 500 Å. Large
13 molecules like *p*-toluidine prefer to be “grafted” inside the mesopores, leading to
14 a dramatically decreased mesoporous pore volume (Figure S3). In contrast, when
15 small molecules such as MeNH₂ are introduced within modified HMIL-121, there
16 is significantly decreased pore volume in both the microporous and mesoporous
17 regions (Figure S3). It is apparent that the large molecules readily react with the
18 anhydrides decorated in the mesopores, while the anhydride groups in the
19 micropores of HMIL-121 are much less accessible to many guests.

20
21
22 To directly characterize the new functionalities introduced via PSM and gain
23 key information on underlying chemistry of the PSM procedures, SSNMR
24 spectroscopy was employed. SSNMR is sensitive to local structure and provides
25 nuclide specific information complementary to that obtained from X-ray
26 diffraction based methods,²⁷⁻²⁸ and is a proven avenue for monitoring PSM
27 processes.²⁹⁻³⁰ Before NMR measurements, any residual reactants that might be

1
2
3
4 occluded inside the MOF pores were removed by thoroughly washing the sample
5
6 with suitable solvents, followed by activation at high temperature and under
7
8 dynamic vacuum. Only the characterization of PSM products obtained by
9
10 acetylation of alcohols and amines, as well as the reaction of the Pt complex with
11
12 anhydride groups anchored inside HMIL-121, is described here in detail to
13
14 illustrate how the anhydride groups act to immobilize guests inside HMIL-121.
15
16
17 The procedures for functionalizing HMIL-121 with other guests are provided in
18
19 the Supporting Information.
20
21
22
23
24
25

26 Acetylation is a reaction that is widely used for producing many industrially
27
28 important compounds, including aspirin, fatty acid esters and macrolides.^{17, 31}
29
30 Acetylation of an alcohol or amine with anhydride results in two products: an ester
31
32 or amide, along with the corresponding acid as a by-product (Figure 3a). Proper
33
34 identification of the ester or amide fragment and corresponding acid group formed
35
36 during PSM is a key step to unambiguously confirming that the acetylation occurs
37
38
39 inside HMIL-121.
40
41
42
43
44
45
46
47
48
49
50
51
52
53
54
55
56
57
58
59
60

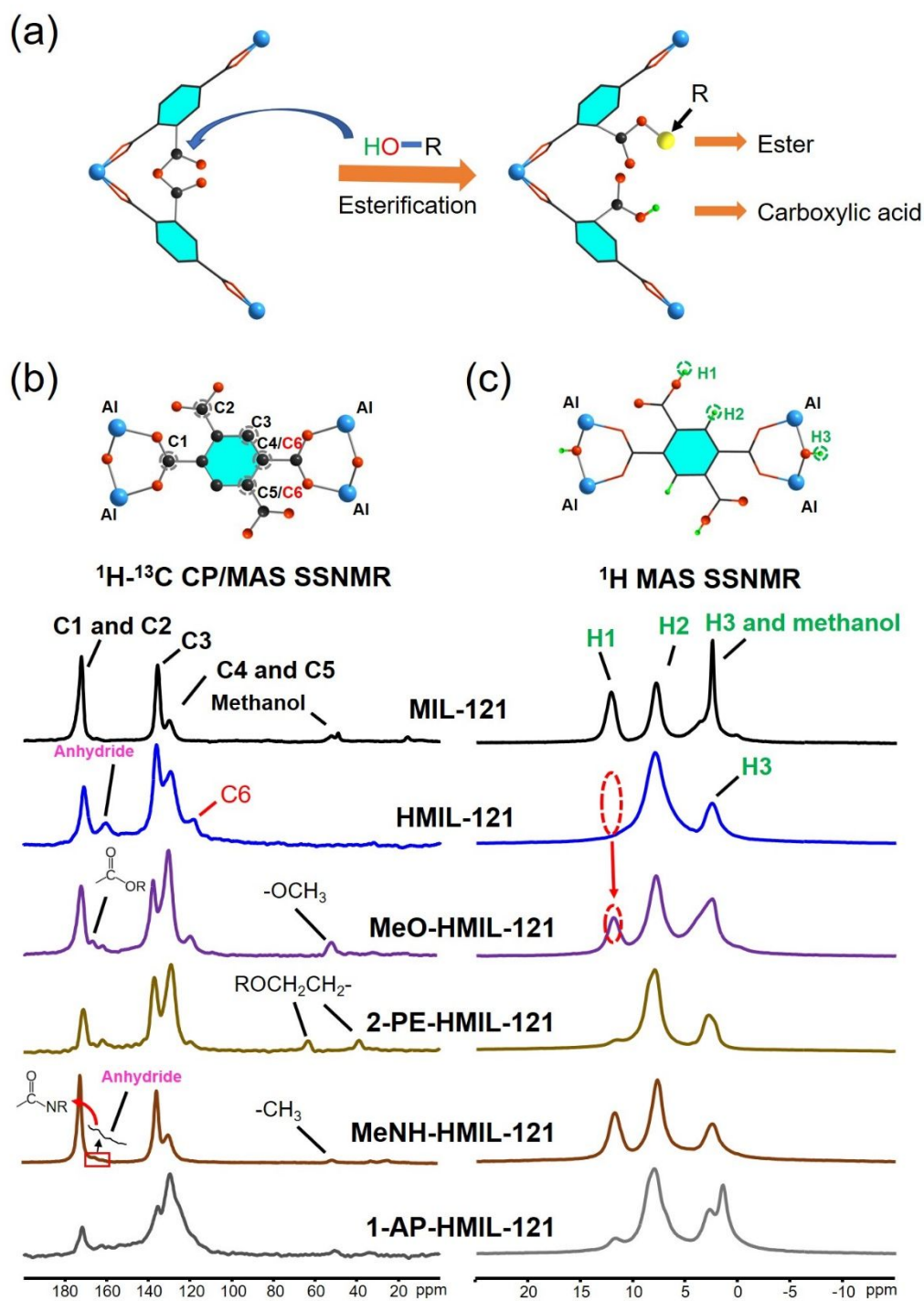


Figure 3. (a) An illustration of the esterification of an anhydride group in HMIL-121 with an alcohol, where oxygen is red, carbon is grey, aluminum is blue, and hydrogen is green. In (b) and (c), the ^{13}C CP/MAS and ^1H MAS SSNMR spectra of MIL-121, HMIL-121 and post-synthetically modified HMIL-121 are shown. All the spectra were obtained at a magnetic field strength of 9.4 T and a spinning speed of 14.0 kHz. In this figure, “2-PE” represents 2-phenylethanol and “1-AP” is shorthand for 1-aminopyrene. A depiction of the BTEC linker

1
2
3
4 with corresponding labels for each unique carbon and hydrogen is shown at the top of each
5 spectral stack.
6
7

8
9 To this end, ^{13}C CP (cross polarization) / MAS (magic angle spinning) and ^1H
10 MAS NMR spectra of MIL-121, HMIL-121, MeO-HMIL-121, 2-PE-HMIL-121,
11 MeNH-HMIL-121 and 1-AP-HMIL-121 were collected, and are shown in Figures
12 3b and 3c. The ^{13}C CP/MAS NMR spectrum of MIL-121 features three main
13 signals. The signal at *ca.* 172 ppm arises from the C1 and C2 sites from the Al-
14 coordinated carboxylate and free carboxylic acid groups. The resonances at *ca.*
15 134.9 and 130.0 ppm originate from the C3, C4 and C5 sites of phenyl carbons
16 (Figure 3b).^{18, 32} The less intense signals at *ca.* 50 ppm belong to residual guest
17 methanol molecules which were subsequently removed during thermal treatment.
18 After the thermolysis procedure is carried out to create hierarchical pores and
19 introducing anhydride functionality, two new resonances appear in the ^{13}C
20 CP/MAS spectrum. The signal at *ca.* 163.0 ppm is assigned to the anhydride
21 groups formed via condensation of two adjacent free carboxylic acid groups,³³⁻³⁴
22 and the other new signal located at *ca.* 123.2 ppm corresponds to the C6 site,
23 which is formed from the C5 and C4 sites that lost their neighboring carboxylate
24 carbon (*i.e.* C1 and C2) during decarboxylation under thermal treatment (Figure
25 3b).
26
27
28
29
30
31
32
33
34
35
36
37
38
39
40
41
42
43
44
45
46
47
48
49
50
51
52
53

54 The ^1H MAS NMR spectrum of MIL121 features three resonances (Figure 3c).
55 The resonance at *ca.* 12 ppm is assigned to the acidic proton on the free COOH
56 groups of the BTEC linker (labeled H1), and the resonance at *ca.* 8 ppm originates
57
58
59
60

1
2
3
4 from the phenyl hydrogens (H2) of the BTEC linker. Several proton signals are
5
6 apparent between 2-6 ppm: the broader and weaker resonance is due to the
7
8 hydroxyl group bridging the adjacent Al centers (H3); the sharper and stronger
9
10 peak is due to adsorbed methanol. After thermal treatment, the H1 resonance
11
12 completely disappears owing to the formation of anhydride groups, suggesting
13
14 that there are no more free carboxylic acid groups inside HMIL-121. As all the
15
16 resonances in both ^{13}C and ^1H SSNMR spectra in MIL-121 and HMIL-121 are
17
18 assigned, any new features appearing in the spectra of post-synthetically modified
19
20 HMIL-121 should originate solely from the new functional moieties introduced
21
22 during PSM.
23
24
25
26
27
28
29

30
31 In the ^{13}C CP/MAS spectrum of the product obtained from PSM of HMIL-121
32
33 via methanol acetylation (termed MeO-MIL-121), there are two new resonances
34
35 in addition to those seen in the spectrum of the pristine HMIL-121. The signal at
36
37 *ca.* 168.5 ppm is assigned to the carbonyl moiety in a phenyl ester, indicating that
38
39 esterification has occurred between anhydride groups in HMIL-121 and the
40
41 methanol guests within the pores. The other resonance at *ca.* 51.0 ppm is due to
42
43 the methoxy group in the resulting methyl ester. Because MeO-HMIL-121 has
44
45 been activated at 150 °C under vacuum for 8 hours, the methoxy group signal
46
47 must exclusively originate from the ester moiety grafted on the MOF, rather than
48
49 from residual guest methanol. The significant decrease in the intensity of the
50
51 resonance at *ca.* 163 ppm due to the anhydride group is also consistent with
52
53 methanol acetylation. ^1H MAS NMR spectra also provide direct evidence of
54
55
56
57
58
59
60

acetylation. Upon reaction with methanol, the H1 resonance reappears, implying that the free carboxylic acid re-forms in MeO-HMIL-121 due to esterification (Figure 3c). Together, ^{13}C CP/MAS and ^1H MAS SSNMR spectra unambiguously confirm that the esterification of methanol with anhydride group has occurred inside HMIL-121.

Incorporation of 2-PE (2-phenylethanol), methylamine and 1-aminopyrene inside HMIL-121 also produced similar spectral features in their respective ^1H - ^{13}C CP/MAS and ^1H MAS NMR spectra, confirming the formation of ester or amide groups and the reformation of free carboxylic acid groups. Other organic molecules including ethanol, aniline, *p*-toluidine, 4-aminobiphenyl and 1,2-ethanedithiol were also grafted into HMIL-121 via reactions with anhydride groups. The experimental details and results regarding these post-synthetically modified HMIL-121 variants can be found in the SI.

Modification of HMIL-121 with a Pt complex.

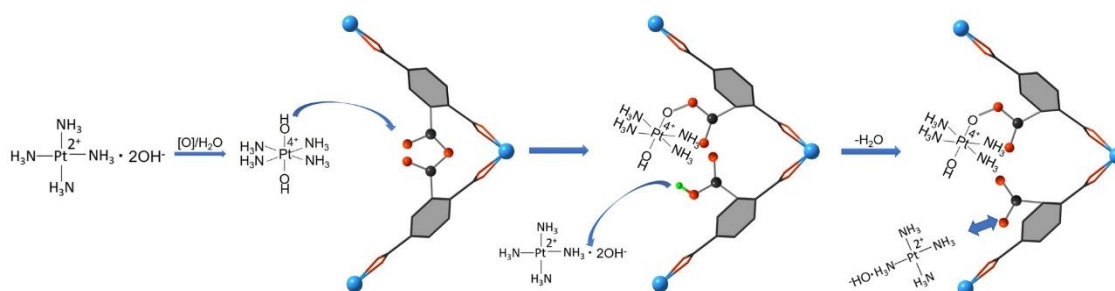


Figure 4. The proposed mechanism of incorporation of the Pt species inside HMIL-121.

Platinum is one of the most widely used noble metals due to its well-known

1
2
3
4 catalytic properties.³⁵⁻³⁶ In contrast to other noble metals, Pt has particularly
5
6 important pharmaceutical applications, as Pt-based drugs are critical agents for
7
8 treating several types of cancers.³⁷⁻³⁸ Square-planar Pt(II)-based drugs and the
9
10 more stable carboxylate platinum(IV) prodrugs based on the Pt(II) precursor are
11
12 used in both research and clinical therapy.³⁹⁻⁴⁰ Carboxylate-functionalized
13
14 platinum(IV) prodrugs are usually obtained by a reaction between anhydride and
15
16 square-planar Pt(II) drugs with oxidizing reagents such as O₂, H₂O₂ or Cl₂.⁴⁰⁻⁴¹
17
18 Keeping these pharmaceutical applications in mind, we have successfully
19
20 introduced Pt(II) and Pt(IV) species into HMIL-121 using a Pt salt,
21
22 tetraammineplatinum(II) hydroxide, Pt(NH₃)₄(OH)₂ as a precursor. The resulting
23
24 material is termed Pt-HMIL-121,
25
26
27
28
29
30
31

32
33 By mixing HMIL-121 with an aqueous solution of Pt(NH₃)₄(OH)₂ at room
34
35 temperature without the need for any catalyst, Pt-HMIL-121 is obtained. The
36
37 product was collected and washed thoroughly by water to remove any residual Pt
38
39 precursor (see details in the SI). To confirm the inclusion of Pt complexes, ¹H-
40
41 ¹⁹⁵Pt BRAIN-CPMG SSNMR experiments were carried out. This particular NMR
42
43 technique enables us to acquire extremely wide ¹⁹⁵Pt spectra.²³ The experimental
44
45 and simulated ¹⁹⁵Pt NMR spectra of Pt(NH₃)₄(OH)₂ and Pt-HMIL-121 are shown
46
47 in Figure S5a along with a more detailed discussion in the caption (page S12 in
48
49 SI). These ¹H-¹⁹⁵Pt CP SSNMR experiments reveal the existence of both a Pt(II)
50
51 and Pt(IV) species in Pt-HMIL-121. The ¹⁹⁵Pt SSNMR results are in excellent
52
53 agreement with XPS analysis (Figure S5b). To further investigate the
54
55
56
57
58
59
60

1
2
3
4 incorporation of two Pt species in HMIL-121, we also carried out ^1H - ^{13}C CP/MAS
5
6 and ^1H MAS SSNMR experiments on Pt-HMIL-121 (Figure S6). As mentioned
7
8 earlier, the signal at 172 ppm in the ^{13}C spectrum of MIL-121 originates from two
9
10 overlapping resonances: C1 from the Al-coordinated carbon atom and C2 from
11
12 the free carboxylate groups. Our previous study³² showed that once the free
13
14 carboxylate groups are doped with extra-framework metal ions, new signals often
15
16 appear on the lower-field side of the peak at 172 ppm, which is due to the C2 site
17
18 of the free COO^- group interacting with the newly-introduced metal ions. In the
19
20 ^{13}C spectrum of Pt-HMIL-121, an extra peak indeed appears at *ca.* 179 ppm as a
21
22 broad shoulder on the low-field side of the 172 ppm peak (Figure S6a) upon PSM,
23
24 confirming the HMIL-121 has indeed incorporated Pt. The breadth of the new ^{13}C
25
26 signal is consistent with ^{195}Pt NMR and XPS results that indicate there is more
27
28 than one Pt species grafted within the MOF. No H1 resonance is observed in the
29
30 ^1H MAS spectrum of Pt-HMIL-121 (Figure S6b), which differs from all other
31
32 HMIL-121 variants modified by organic species, suggesting that the reactions
33
34 more complicated than simple acetylation involving Pt have taken place.
35
36
37
38
39
40
41
42
43
44
45

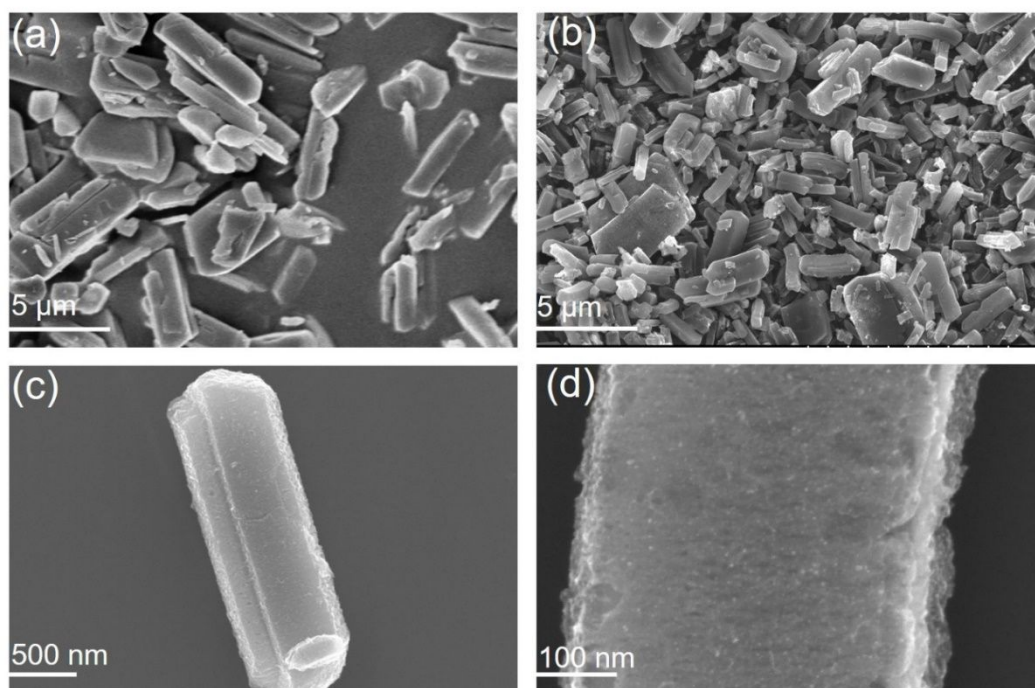
46
47 Based on our multinuclear SSNMR and XPS results, a mechanism can
48
49 proposed for this Pt incorporation in HMIL-121. First, Pt(II) in square planar
50
51 $\text{Pt}(\text{NH}_3)_4(\text{OH})_2$ is oxidized to octahedral Pt(IV) by molecular oxygen dissolved in
52
53 water, resulting in the addition of two hydroxyl groups to the Pt center (Figure
54
55 4).⁴⁰⁻⁴¹ This octahedral Pt(IV) complex is then bound to a carboxylate groups after
56
57 reacting with an anhydride group of HMIL-121.⁴¹ The incorporation of the
58
59
60

1
2
3
4 octahedral Pt(IV) complex is accompanied by the formation of free carboxylic
5
6 acid groups that subsequently react with basic $\text{Pt}(\text{NH}_3)_4(\text{OH})_2$, resulting in
7
8 grafting the corresponding square-planar Pt(II) species on HMIL-121 (Figure 4).
9
10 This acid-base reaction is further confirmed by the change in pH during the
11
12 experiment – the initial aqueous solution of $\text{Pt}(\text{NH}_3)_4(\text{OH})_2$ has a pH value of 10.0
13
14 and gradually becomes neutral after mixing with HMIL-121, providing evidence
15
16 that a neutralization reaction has occurred. This proposed route also explains the
17
18 absence of an H1 signal in the ^1H MAS NMR spectrum of Pt-HMIL-121 (Figure
19
20 S6b). The success in incorporation of Pt(II)/Pt(IV) species in the MOF indicates
21
22 that the PSM protocol described here has potential to be used for drug delivery.
23
24 More research along this line is needed.
25
26
27
28
29
30
31
32

33 **The electrocatalytic activity towards ORR**

34
35
36
37 As mentioned earlier, elemental Pt has considerable practical importance in
38
39 catalysis. Therefore, Pt-HMIL-121 obtained via PSM was used to fabricate a
40
41 MOF-derived hierarchical porous carbon network with embedded Pt nano-
42
43 particles (NPs) as an electrocatalyst for the oxygen reduction reaction (ORR).
44
45 Fuel cells and metal-air batteries are very promising candidates for
46
47 environmentally sustainable energy sources, where ORR plays a key role in
48
49 determining their electrical energy conversion.⁴²⁻⁴³ Currently, Pt-based cathodes
50
51 are still the most efficient materials for catalyzing ORR.⁴³ Due to the high cost of
52
53 Pt, developing electrocatalysts of low Pt content without sacrificing performance
54
55
56
57
58
59
60

1
2
3
4 is critical to achieving large scale industrial production for electric vehicles and
5
6 other applications involving ORR.⁴³ Recently, MOF-derived carbon materials
7
8 have attracted tremendous attention due to their inherently high surface areas and
9
10 porosity compared to their parent MOF precursors, leading to high exposure and
11
12 easy accessibility of the active sites.^{11, 44} In addition, the resulting MOF-derived
13
14 carbon materials have much better electrical conductivity and higher
15
16 thermal/chemical stability compared to their parent MOFs, making them an ideal
17
18 host for fabricating highly dispersed metal doped electrocatalysts.^{11, 45}
19
20
21
22
23
24



48
49 **Figure 5.** SEM images of Pt-HMIL-121 (a) along with Pt-HMIL-121-900 samples at several
50 different scales (b, c, d).
51

52
53
54 Pt-HMIL-121 was pyrolyzed by heat treatment at 900°C for 1 hour under Ar
55 atmosphere, followed by hydrochloric acid leaching to remove the unstable Al
56 species (see details in the SI). The resulting catalyst is termed Pt-HMIL-121-900,
57
58
59
60

1
2
3
4 which is composed of uniformly dispersed Pt nanoparticles embedded in the
5
6 porous carbon matrix. During pyrolysis, the grafted Pt complexes decompose,
7
8 generating the reduced metallic Pt NPs. The HMIL-121 substrate is carbonized
9
10 and converted into the conductive Al-doped porous carbon. The Pt-HMIL-121-
11
12 900 material with highly dispersed Pt NPs was thus fabricated. Before testing the
13
14 electrochemical catalytic performance, the morphology of the precursor (Pt-
15
16 HMIL-121) and the catalyst (Pt-HMIL-121-900) was carefully examined by
17
18 scanning electron microscopy (SEM). As shown in Figure 5, the SEM images at
19
20 different scales indicate that Pt-HMIL-121-900 remains as parallelepiped-shaped
21
22 crystals, which are similar to those of parent Pt-HMIL-121. After high
23
24 temperature treatment at 900 °C, the Pt-HMIL-121-900 crystal sizes became
25
26 smaller than those of HMIL-121 (Figures S1d and 5a/b), which is a common
27
28 phenomenon in carbonized MOFs due to the loss of most H and O elements.⁴⁶
29
30 The crystal faces of Pt-HMIL-121-900 are decorated with prominent mesopores,
31
32 suggesting the existence of a hierarchical structure with a large average pore size.
33
34 The differences in surface area and hierarchical pore between Pt-HMIL-121 and
35
36 Pt-HMIL-121-900 were further characterized by N₂ sorption tests. The two
37
38 samples both show the same type IV isotherms with hysteresis loops, which are
39
40 similar to that of HMIL-121 (Figure S7), suggesting the existence of both
41
42 mesopores and micropores. The calculated BET surface area for Pt-HMIL-121 is
43
44 411.0 m²/g, which is less than that of HMIL-121 (887.6 m²/g) due to the steric
45
46 hindrance of the incorporated Pt complex species within the pore channels. In
47
48
49
50
51
52
53
54
55
56
57
58
59
60

contrast, the BET surface area for Pt-HMIL-121-900 reaches as high as 2866 m²/g. This value is one of the highest reported BET surface areas among pyrolytic MOFs,^{45, 47} suggesting Pt-HMIL-121-900 has potential to provide sufficient exposure of the Pt sites, which can facilitate mass transport during the ORR.

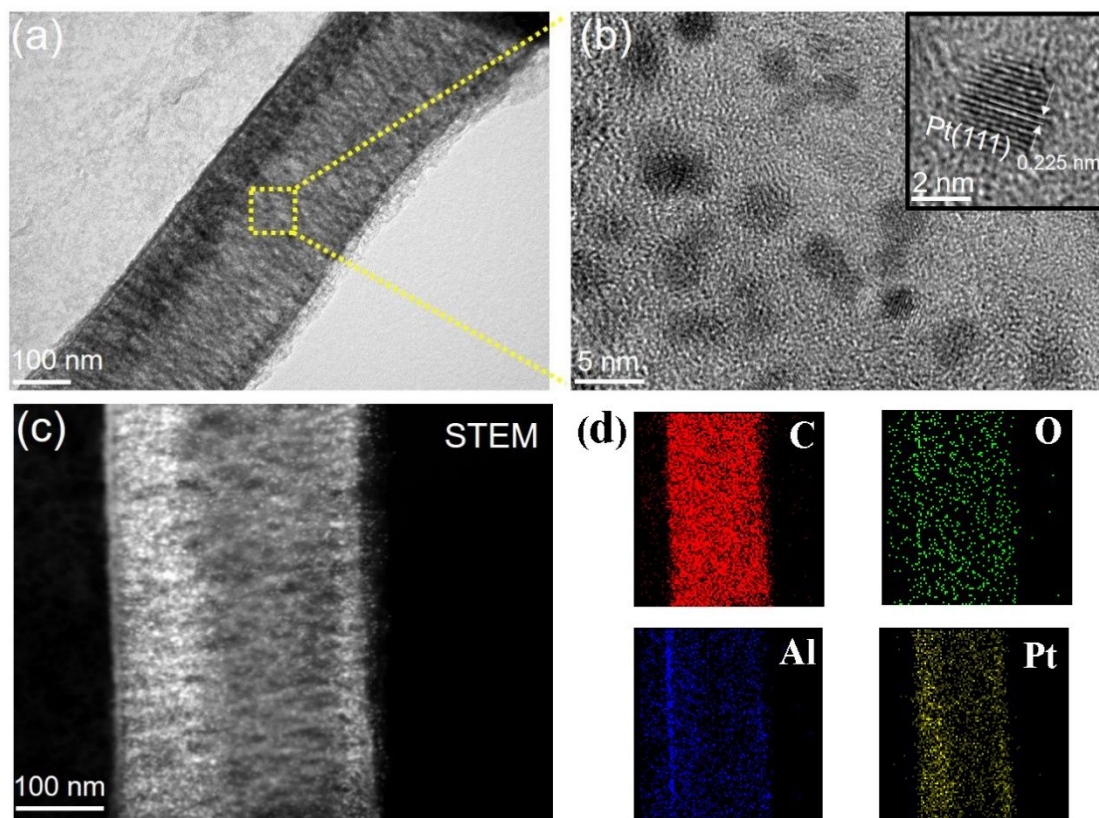


Figure 6. TEM and HRTEM images of Pt-HMIL-121-900. Scale bars are 100 nm in (a), 5 nm in (b) and 2 nm for the inset of (b). The STEM image (c) and element maps (d) of Pt-HMIL-121-900 are also shown.

Transmission electron microscopy (TEM) images show more details of the Pt-HMIL-121-900 sample. From Figure 6a, it can be seen that Pt-HMIL-121 is converted into an Al-doped porous carbon network decorated with Pt NPs dispersed both on the surface and in the pores of Pt-HMIL-121-900 substrate. The

1
2
3
4 high-resolution TEM image clearly shows uniform Pt particles with an average
5
6 size of 2.5 nm (Figure 6b), suggesting that the Pt particle size is controlled by the
7
8 nanopore trapping effect, which prevents Pt NPs from diffusion and therefore
9
10 aggregation during heating; this leads to excellent stability. The lattice distance of
11
12 crystalline Pt NPs is measured from the HRTEM image and given in the inset of
13
14 Figure 6b. The periodic fringe spaces are 0.225 nm, which agrees well with the
15
16 interplanar d value for (111) planes of crystalline Pt.⁴⁸ Elemental mapping
17
18 analysis (Figures 6c-d) demonstrates that Pt-HMIL-121-900 is composed of C, O,
19
20 Al and Pt, with Pt and Al well dispersed in the porous carbon matrix. The Pt
21
22 loading determined by ICP-OES (inductively coupled plasma - optical emission
23
24 spectroscopy) is 7.0 wt% of Pt in Pt-HMIL-121-900. The PXRD patterns of Pt-
25
26 HMIL-121 and Pt-HMIL-121-900 have significant differences and are shown in
27
28 Figure S8. After pyrolysis, the diffraction peaks of HMIL-121 disappear, and
29
30 well-defined crystalline Pt reflections appear in the PXRD pattern of Pt-HMIL-
31
32 121-900 (Figure S8). The porous carbon is generated from the decomposition of
33
34 the host HMIL-121. During high temperature pyrolysis, most of the hydrogen,
35
36 oxygen and carbon elements are vaporized, resulting in a Pt-doped hierarchically
37
38 porous carbon material.
39
40
41
42
43
44
45
46
47
48
49
50
51
52
53
54
55
56
57
58
59
60

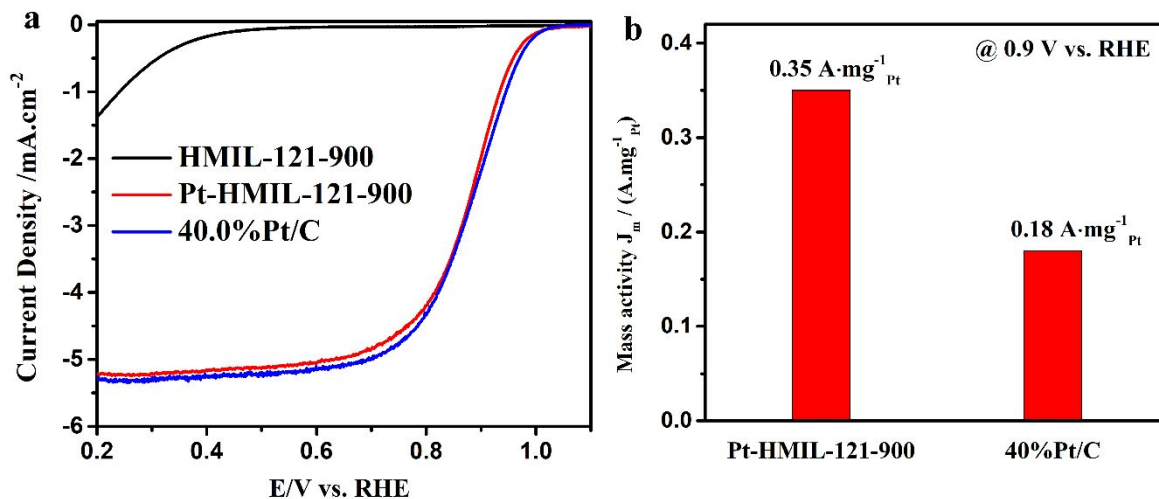


Figure 7. (a) Linear scan voltammogram (LSV) curves for the electrocatalysts of Pt-HMIL-121-900, HMIL-121-900, and 40.0%Pt/C catalysts in O_2 -saturated 0.1 M HClO_4 solution at room temperature (rotating speed of 1600 rpm, sweep rate $10\text{mV}\cdot\text{s}^{-1}$). (b) The mass activity at 0.9 V (vs. RHE) for Pt-HMIL-121-900 and commercial 40 % Pt/C catalysts.

The electrochemical performance of Pt-HMIL-121-900 has been evaluated for ORR and compared with the performances of pyrolytic HMIL-121 (termed as HMIL-121-900) and the state-of-the-art commercial Pt/C catalyst (40.0 wt % Pt and termed as 40 % Pt/C catalyst). Figure 7a presents the linear scan voltammogram (LSV) curves for Pt-HMIL-121-900, HMIL-121-900 and 40% Pt/C catalysts obtained in a O_2 -saturated 0.1 M HClO_4 electrolyte at a rotating speed of 1600 rpm. Pt-HMIL-121-900 displays a significantly positively-shifted ORR onset potential of 1.04 V (vs. RHE) and a higher current density of $5.3 \text{ mA}\cdot\text{cm}^{-2}$ compared to the corresponding values of HMIL-121-900. The kinetic currents at 0.9 V for the studied electrocatalysts obtained from the Koutecky-Levich equation were used to derive Pt mass activities (Figure 7b). For the fresh catalysts, Pt-HMIL-121-900 exhibits a mass activity of $0.35 \text{ A}\cdot\text{mg}^{-1}_{\text{Pt}}$ at 0.9 V,

1
2
3
4 which is about two times higher than that of commercial 40% Pt/C catalyst (0.18
5
6 $A \cdot mg^{-1}_{Pt}$). The result indicates that Pt-HMIL-121-900 with an ultra-low Pt loading
7
8 of 7.0 wt % exhibits excellent catalytic performance in the ORR, and has a much
9
10 higher ORR mass activity compared to that of the commercial Pt/C catalyst. The
11
12 combination of highly dispersed Pt NPs with appropriate particle sizes and the
13
14 hierarchically porous carbon matrix (Pt-HMIL-121-900) derived from MOF-
15
16 based material results in an excellent ORR activity. This work demonstrates that
17
18 the hierarchically porous HMIL-121 MOF functionalized with anhydride groups
19
20 has great potential for fabrication of efficient Pt doped electrocatalysts for ORR,
21
22 as well as for other energy conversion reactions involving Pt metal.
23
24
25
26
27
28
29

30 **Conclusion**

31
32
33
34 In this work, we have demonstrated that a hierarchically porous MOF
35
36 decorated with anhydride groups is a novel platform for PSM of MOFs. It exhibits
37
38 excellent reactivity towards covalently grafting various organic species as well as
39
40 Pt(IV)/Pt(II) complexes on the pore walls. The ability of this protocol to
41
42 immobilize Pt(II)/Pt(IV) species inside MOFs has important implications for drug
43
44 delivery and fabrication of Pt-based heterogenous catalysts. The combination of
45
46 the highly active anhydride group and the hierarchical pore structure of the MOF
47
48 makes the approach described a novel and very effective protocol for PSM of
49
50 MOFs. This strategy opens a novel avenue for introducing multiple chemical
51
52 functionalities inside MOFs, and also offers a tunable platform for metalation of
53
54
55
56
57
58
59
60

1
2
3
4 MOFs with noble metals. Furthermore, the facts that the precursor for PSM (*i.e.*
5
6 the hierarchically porous MOF decorated with anhydride groups) can be easily
7
8 prepared from simple low-cost carboxylate-based MOFs via thermolysis in a
9
10 controlled fashion and that in addition to MIL-121, many important MOFs either
11
12 have or can be easily functionalized to form free carboxylic acid groups make this
13
14 new PSM method widely applicable for diverse applications. Looking forward,
15
16 covalent organic frameworks (COFs) can be functionalized via carboxylic
17
18 groups,⁴⁹⁻⁵⁰ which suggests that the protocol described here can be expanded to
19
20 include PSM of COFs and other related porous organic polymers.
21
22
23
24
25
26
27
28
29
30

31 **Acknowledgements.**

32
33
34
35 Y.H., X.S. and M.S.W. thank the Natural Science and Engineering Research
36
37 Council (NSERC) of Canada for Discovery Grants. X.S. also thanks Canada
38
39 Research Chair (CRC) Program, Canada Foundation for Innovation (CFI) and
40
41 Ontario Research Fund (ORF). The National Natural Science Foundation of
42
43 China is acknowledged by Z.S. (NSFC21905179), J.L. (NSFC21506189) and
44
45 Y.G. (NSFC51472021).
46
47
48
49
50

51 **Competing Interests.**

52
53
54
55 The authors declare no competing interests.
56
57
58

59 **Supporting Information.**

1
2
3
4 Details on sample preparation, additional PXRD patterns, SEM images, N₂
5
6 adsorption isotherms, ¹³C CP/MAS and ¹H MAS spectra, ¹H-¹⁹⁵Pt BRAIN-CPMG
7
8 SSNMR spectra and ¹⁹⁵Pt CS tensor parameters, XPS and TGA data can be found
9
10 in the Supplementary Information.
11
12
13

14 15 **Author Information.**

16
17
18
19 [†]S. C. and Z. S. contributed equally to this work.
20
21

22 23 **References.**

- 24
25
26 1. Furukawa, H.; Cordova, K. E.; O’Keeffe, M.; Yaghi, O. M., The chemistry
27
28 and applications of metal-organic frameworks. *Science* **2013**, *341* (6149),
29
30 1230444.
31
32
33 2. Zhou, H.-C.; Long, J. R.; Yaghi, O. M., Introduction to Metal–Organic
34
35 Frameworks. *Chem. Rev.* **2012**, *112* (2), 673-674.
36
37
38 3. Chen, M.; Chen, S.; Chen, W.; Lucier, B. E. G.; Zhang, Y.; Zheng, A.; Huang,
39
40 Y., Analyzing Gas Adsorption in an Amide-Functionalized Metal Organic
41
42 Framework: Are the Carbonyl or Amine Groups Responsible? *Chem. Mater.* **2018**,
43
44 *30* (11), 3613-3617.
45
46
47 4. Yu, J.; Xie, L.-H.; Li, J.-R.; Ma, Y.; Seminario, J. M.; Balbuena, P. B., CO₂
48
49 capture and separations using MOFs: computational and experimental studies.
50
51
52 *Chem. Rev.* **2017**, *117* (14), 9674-9754.
53
54
55
56 5. Park, T.-H.; Hickman, A. J.; Koh, K.; Martin, S.; Wong-Foy, A. G.; Sanford,
57
58 M. S.; Matzger, A. J., Highly dispersed palladium (II) in a defective metal–
59
60

-
- 1
2
3
4 organic framework: application to C–H activation and functionalization. *J. Am.*
5
6 *Chem. Soc.* **2011**, *133* (50), 20138-20141.
- 7
8
9 6. Jiang, H.-L.; Akita, T.; Ishida, T.; Haruta, M.; Xu, Q., Synergistic catalysis of
10
11 Au@ Ag core– shell nanoparticles stabilized on metal– organic framework. *J. Am.*
12
13 *Chem. Soc.* **2011**, *133* (5), 1304-1306.
- 14
15
16
17 7. Dhakshinamoorthy, A.; Garcia, H., Catalysis by metal nanoparticles
18
19 embedded on metal–organic frameworks. *Chem. Soc. Rev.* **2012**, *41* (15), 5262-
20
21 5284.
- 22
23
24
25 8. Hu, Z.; Deibert, B. J.; Li, J., Luminescent metal–organic frameworks for
26
27 chemical sensing and explosive detection. *Chem. Soc. Rev.* **2014**, *43* (16), 5815-
28
29 5840.
- 30
31
32
33 9. Horcajada, P.; Serre, C.; Vallet-Regí, M.; Sebban, M.; Taulelle, F.; Férey, G.,
34
35 Metal–organic frameworks as efficient materials for drug delivery. *Angew. Chem.*
36
37 **2006**, *118* (36), 6120-6124.
- 38
39
40
41 10. Horcajada, P.; Chalati, T.; Serre, C.; Gillet, B.; Sebrie, C.; Baati, T.; Eubank,
42
43 J. F.; Heurtaux, D.; Clayette, P.; Kreuz, C., Porous metal-organic-framework
44
45 nanoscale carriers as a potential platform for drug delivery and imaging. *Nat.*
46
47 *Mater.* **2010**, *9* (2), 172.
- 48
49
50
51 11. Zhao, Y.; Song, Z.; Li, X.; Sun, Q.; Cheng, N.; Lawes, S.; Sun, X., Metal
52
53 organic frameworks for energy storage and conversion. *Energy Storage Mater.*
54
55 **2016**, *2*, 35-62.
- 56
57
58
59 12. Jiang, J.; Zhao, Y.; Yaghi, O. M., Covalent chemistry beyond molecules. *J.*
60

1
2
3
4 *Am. Chem. Soc.* **2016**, *138* (10), 3255-3265.

5
6
7 13. Cohen, S. M., The postsynthetic renaissance in porous solids. *J. Am. Chem.*
8
9 *Soc.* **2017**, *139* (8), 2855-2863.

10
11
12 14. Cohen, S. M., Postsynthetic methods for the functionalization of metal–
13
14 organic frameworks. *Chem. Rev.* **2011**, *112* (2), 970-1000.

15
16
17 15. Moghadam, P. Z.; Li, A.; Wiggin, S. B.; Tao, A.; Maloney, A. G.; Wood, P.
18
19 A.; Ward, S. C.; Fairen-Jimenez, D., Development of a Cambridge Structural
20
21 Database subset: a collection of metal–organic frameworks for past, present, and
22
23 future. *Chem. Mater.* **2017**, *29* (7), 2618-2625.

24
25
26
27 16. Evans, J. D.; Sumby, C. J.; Doonan, C. J., Post-synthetic metalation of metal–
28
29 organic frameworks. *Chem. Soc. Rev.* **2014**, *43* (16), 5933-5951.

30
31
32 17. Carey, F. A.; Sundberg, R. J., *Advanced organic chemistry: part A: structure*
33
34 *and mechanisms*. Springer Science & Business Media: 2007.

35
36
37 18. Volkringer, C.; Loiseau, T.; Guillou, N.; Férey, G. r.; Haouas, M.; Taulelle,
38
39 F.; Elkaim, E.; Stock, N., High-Throughput Aided Synthesis of the Porous Metal–
40
41 Organic Framework-Type Aluminum Pyromellitate, MIL-121, with Extra
42
43 Carboxylic Acid Functionalization. *Inorg. Chem.* **2010**, *49* (21), 9852-9862.

44
45
46
47 19. Chen, S.; Mukherjee, S.; Lucier, B. E.; Guo, Y.; Wong, Y. T. A.; Terskikh, V.
48
49 V.; Zaworotko, M. J.; Huang, Y., Cleaving Carboxyls: Understanding Thermally
50
51 Triggered Hierarchical Pores in the Metal-Organic Framework MIL-121. *J. Am.*
52
53 *Chem. Soc.* **2019**, *141* (36), 14257-14271.

54
55
56
57 20. Hayashi, S.; Hayamizu, K., Shift references in high-resolution solid-state
58
59
60

1
2
3
4 NMR. *Bull. Chem. Soc. Jpn.* **1989**, *62* (7), 2429-2430.

5
6 21. Hayashi, S.; Hayamizu, K., Chemical shift standards in high-resolution solid-
7 state NMR (1) ^{13}C , ^{29}Si , and ^1H nuclei. *Bull. Chem. Soc. Jpn.* **1991**, *64* (2), 685-
8 687.

9
10 22. Harris, R. K.; Becker, E. D.; Cabral de Menezes, S. M.; Goodfellow, R.;
11 Granger, P., NMR nomenclature. Nuclear spin properties and conventions for
12 chemical shifts (IUPAC recommendations 2001). *Pure Appl. Chem.* **2001**, *73* (11),
13 1795-1818.

14
15 23. Harris, K. J.; Lupulescu, A.; Lucier, B. E.; Frydman, L.; Schurko, R. W.,
16 Broadband adiabatic inversion pulses for cross polarization in wideline solid-state
17 NMR spectroscopy. *J. Magn. Reson.* **2012**, *224*, 38-47.

18
19 24. Tang, J. A.; O'Dell, L. A.; Aguiar, P. M.; Lucier, B. E.; Sakellariou, D.;
20 Schurko, R. W., Application of static microcoils and WURST pulses for solid-
21 state ultra-wideline NMR spectroscopy of quadrupolar nuclei. *Chem. Phys. Lett.*
22 **2008**, *466* (4), 227-234.

23
24 25. O'Dell, L. A., The WURST kind of pulses in solid-state NMR. *Solid State*
25 *Nucl. Magn. Reson.* **2013**, *55*, 28-41.

26
27 26. Mayrhofer, K.; Strmcnik, D.; Blizanac, B.; Stamenkovic, V.; Arenz, M.;
28 Markovic, N., Measurement of oxygen reduction activities via the rotating disc
29 electrode method: From Pt model surfaces to carbon-supported high surface area
30 catalysts. *Electrochim. Acta* **2008**, *53* (7), 3181-3188.

31
32 27. Lucier, B. E. G.; Chen, S.; Huang, Y., Characterization of Metal–Organic
33
34
35
36
37
38
39
40
41
42
43
44
45
46
47
48
49
50
51
52
53
54
55
56
57
58
59
60

1
2
3
4 Frameworks: Unlocking the Potential of Solid-State NMR. *Acc. Chem. Res.* **2018**,
5
6
7 *51* (2), 319-330.

8
9 28. Chen, S.; Lucier, B. E. G.; Boyle, P. D.; Huang, Y., Understanding The
10
11 Fascinating Origins of CO₂ Adsorption and Dynamics in MOFs. *Chem. Mater.*
12
13
14 **2016**, *28* (16), 5829-5846.

15
16
17 29. Morris, W.; Doonan, C. J.; Yaghi, O. M., Postsynthetic modification of a
18
19 metal–organic framework for stabilization of a hemiaminal and ammonia uptake.
20
21
22 *Inorg. Chem.* **2011**, *50* (15), 6853-6855.

23
24
25 30. Ahnfeldt, T.; Gunzelmann, D.; Loiseau, T.; Hirsemann, D.; Senker, J. r.; Férey,
26
27 G.; Stock, N., Synthesis and modification of a functionalized 3D open-framework
28
29 structure with MIL-53 topology. *Inorg. Chem.* **2009**, *48* (7), 3057-3064.

30
31
32 31. Otera, J.; Nishikido, J., *Esterification: methods, reactions, and applications*.
33
34
35 John Wiley & Sons: 2009.

36
37
38 32. Chen, S.; Lucier, B. E. G.; Luo, W.; Xie, X.; Feng, K.; Chan, H.; Terskikh, V.
39
40 V.; Sun, X.; Sham, T.-K.; Workentin, M. S., Loading across the Periodic Table:
41
42 Introducing 14 Different Metal Ions To Enhance Metal–Organic Framework
43
44 Performance. *ACS Appl. Mater. Interfaces* **2018**, *10* (36), 30296-30305.

45
46
47 33. Ragon, F.; Campo, B.; Yang, Q.; Martineau, C.; Wiersum, A. D.; Lago, A.;
48
49 Guillerm, V.; Hemsley, C.; Eubank, J. F.; Vishnuvarthan, M., Acid-functionalized
50
51 UiO-66 (Zr) MOFs and their evolution after intra-framework cross-linking:
52
53 structural features and sorption properties. *J. Mater. Chem. A* **2015**, *3* (7), 3294-
54
55
56
57
58
59
60 3309.

-
- 1
2
3
4 34. Reimer, N.; Gil, B.; Marszalek, B.; Stock, N., Thermal post-synthetic
5
6 modification of Al-MIL-53-COOH: systematic investigation of the
7
8 decarboxylation and condensation reaction. *CrystEngComm* **2012**, *14* (12), 4119-
9
10 4125.
11
12
13
14 35. Periana, R. A.; Taube, D. J.; Gamble, S.; Taube, H.; Satoh, T.; Fujii, H.,
15
16 Platinum catalysts for the high-yield oxidation of methane to a methanol
17
18 derivative. *Science* **1998**, *280* (5363), 560-564.
19
20
21
22 36. Labinger, J. A., Platinum-catalyzed C-H functionalization. *Chem. Rev.* **2016**,
23
24 *117* (13), 8483-8496.
25
26
27 37. Zheng, Y.-R.; Suntharalingam, K.; Johnstone, T. C.; Lippard, S. J.,
28
29 Encapsulation of Pt (IV) prodrugs within a Pt (II) cage for drug delivery. *Chem.*
30
31 *Sci.* **2015**, *6* (2), 1189-1193.
32
33
34
35 38. Wong, E.; Giandomenico, C. M., Current status of platinum-based antitumor
36
37 drugs. *Chem. Rev.* **1999**, *99* (9), 2451-2466.
38
39
40 39. Yap, S. Q.; Chin, C. F.; Thng, H.; Hwee, A.; Pang, Y. Y.; Ho, H. K.; Ang, W.
41
42 H., Finely Tuned Asymmetric Platinum (IV) Anticancer Complexes: Structure-
43
44 Activity Relationship and Application as Orally Available Prodrugs.
45
46 *ChemMedChem* **2017**, *12* (4), 300-311.
47
48
49
50 40. Wilson, J. J.; Lippard, S. J., Synthetic methods for the preparation of platinum
51
52 anticancer complexes. *Chem. Rev.* **2013**, *114* (8), 4470-4495.
53
54
55
56 41. Chin, C. F.; Tian, Q.; Setyawati, M. I.; Fang, W.; Tan, E. S. Q.; Leong, D. T.;
57
58 Ang, W. H., Tuning the activity of platinum (IV) anticancer complexes through
59
60

1
2
3
4 asymmetric acylation. *J. Med. Chem.* **2012**, *55* (17), 7571-7582.

5
6
7 42. Dai, L.; Xue, Y.; Qu, L.; Choi, H.-J.; Baek, J.-B., Metal-free catalysts for
8 oxygen reduction reaction. *Chem. Rev.* **2015**, *115* (11), 4823-4892.

9
10
11 43. Nie, Y.; Li, L.; Wei, Z., Recent advancements in Pt and Pt-free catalysts for
12 oxygen reduction reaction. *Chem. Soc. Rev.* **2015**, *44* (8), 2168-2201.

13
14
15 44. Cao, X.; Tan, C.; Sindoro, M.; Zhang, H., Hybrid micro-/nano-structures
16 derived from metal–organic frameworks: preparation and applications in energy
17 storage and conversion. *Chem. Soc. Rev.* **2017**, *46* (10), 2660-2677.

18
19
20 45. Liang, Z.; Qu, C.; Xia, D.; Zou, R.; Xu, Q., Atomically dispersed metal sites
21 in MOF-based materials for electrocatalytic and photocatalytic energy conversion.
22 *Angew. Chem.* **2018**, *57*, 9604-9633.

23
24
25 46. Zhang, H.; Hwang, S.; Wang, M.; Feng, Z.; Karakalos, S.; Luo, L.; Qiao, Z.;
26 Xie, X.; Wang, C.; Su, D., Single atomic iron catalysts for oxygen reduction in
27 acidic media: particle size control and thermal activation. *J. Am. Chem. Soc.* **2017**,
28 *139* (40), 14143-14149.

29
30
31 47. Indra, A.; Song, T.; Paik, U., Metal organic framework derived materials:
32 Progress and prospects for the energy conversion and storage. *Adv. Mater.* **2018**,
33 *30* (39), 1705146.

34
35
36 48. Guo, X.; Li, L.; Zhang, X.; Chen, J., Platinum Nanoparticles Encapsulated in
37 Nitrogen-Doped Mesoporous Carbons as Methanol-Tolerant Oxygen Reduction
38 Electrocatalysts. *ChemElectroChem* **2015**, *2* (3), 404-411.

39
40
41 49. Lu, Q.; Ma, Y.; Li, H.; Guan, X.; Yusran, Y.; Xue, M.; Fang, Q.; Yan, Y.;

1
2
3
4 Qiu, S.; Valtchev, V., Postsynthetic Functionalization of Three-Dimensional
5
6 Covalent Organic Frameworks for Selective Extraction of Lanthanide Ions.
7
8
9 *Angew. Chem. Int. Ed.* **2018**, *57* (21), 6042-6048.

10
11 50. Guo, L.; Jia, S.; Diercks, C. S.; Yang, X.; Alshimmri, S. A.; Yaghi, O. M.,
12
13 Amidation, Esterification, and Thioesterification of a Carboxyl-Functionalized
14
15 Covalent Organic Framework. *Angew. Chem. Int. Ed.* **2020**, *59* (5), 2023-2027.
16
17
18
19
20
21
22
23
24
25
26
27
28
29
30
31
32
33
34
35
36
37
38
39
40
41
42
43
44
45
46
47
48
49
50
51
52
53
54
55
56
57
58
59
60

1
2
3
4 TOC image:
5
6
7

